Effects of margin-parallel shortening and density contrasts on back-arc extension during subduction: Experimental insights and possible application to Anatolia

Lena Driehaus, Thierry Nalpas, Peter Robert Cobbold, B. Gelabert, F. Sabat

Effects of margin-parallel shortening and density contrasts on back-arc extension during subduction: Experimental insights and possible application to Anatolia

L. Driehaus [a, b], T. Nalpas [a]*, P.R. Cobbold [a], B. Gelabert [c], F. Sàbat [b]

a Géosciences Rennes, UMR 6118, CNRS, Université de Rennes 1, Campus de Beaulieu, 35042 Rennes Cedex, France.

b Departament de Geodinàmica i Geofísica, Facultat de Geologia, Universitat de Barcelona (UB) C/ Martí i Franquès s/n, 08028-Barcelona, Spain.

c Departament de Ciències de la Terra, Universitat de les Illes Balears (UIB) Ctra. De Valldemossa, km 7.5, 07122 Balears, Spain.

***** Corresponding author. Tel.: (34)934035914

E-mail address: lena.driehaus@univ-rennes1.fr

Keywords: Analogue Modelling, Subduction, Back-Arc Extension, Anatolia.

ABSTRACT

So as to investigate the parameters influencing subduction and back-arc extension, we have done three series of laboratory experiments (32 in all) on physical models. Each

model consisted of adjacent oceanic and continental plates, floating on an asthenosphere. In experiments of Series A, a wide rigid piston, moving horizontally, controlled the rate of convergence of the oceanic and continental plates, whereas, in Series B or C, a wide or narrow piston produced lateral compression, parallel to the continent-ocean boundary (COB) and perpendicular to the subduction direction. The parameters that we tested were (1) the velocity of plate convergence (Series A), (2) the width of the compressing piston (Series B and C), and (3) the density ratio between oceanic and continental plates (Series B and C). This density ratio was a key factor. For a ratio of 1.4, the amount of extension in the continental plate increased regularly throughout time; for a ratio of 1.3, the extension remained small, until the piston stopped moving laterally; and for a ratio of 1.1, there was little or no extension. The width of the compressing piston had a smaller effect, although a narrow piston provided more space, into which the continental plate could extend.

One possible application of our models is to Anatolia. Despite similar geological settings, the areas north of the Hellenic and Cyprus subduction zones differ, in that extension is large in the former and much smaller in the latter. We suggest that one of the main driving forces for Aegean extension may have been a high density ratio between subducting oceanic lithosphere and a Hellenic-Balkanic upper plate.

1. Introduction

It is a common observation that continental margins next to subduction zones have undergone horizontal extension in directions perpendicular to the margins. According to Mantovani et al., (2001) and Heuret and Lallemand (2005), there are three main models for explaining how subduction can lead to such back-arc extension.

1. In the slab-pull model, back-arc extension results from the negative buoyancy of the subducting lithosphere with respect to the surrounding mantle (e.g. Molnar and Atwater, 1978; Dewey, 1980; Malinverno and Ryan, 1986; Royden, 1993). Several series of physical experiments have tested this model (Becker et al., 1999; Regard el al., 2003, 2005 and 2008; Faccenna et al., 1996, 1999, 2004 and 2006; Heuret and Lallemand, 2005; Heuret et al., 2007; Funiciello et al., 2008; Guillaume et al., 2009).

2. In the corner flow model, back-arc extension results from mantle flow in the asthenospheric wedge overlying the subducting slab (e.g. Toksoz and Bird, 1977; Toksoz and Hsui, 1978; Jurdy and Stefanick, 1983; Rodkin and Rodnikov, 1996). Several series of physical experiments have tested this model also (Funiciello et al., 2004; Heuret and Lallemand, 2005; Regard et al., 2008)

3. In the sea anchor model, back-arc extension results from landward motion of the overriding plate with respect to the subducting plate, which encounters viscous resistance in the asthenosphere (e.g. Scholz and Campos, 1995). Once again, several series of physical experiments have tested this model (Faccenna et al., 1996; Heuret and Lallemand, 2005).

In other models (Mantovani, 1997; Mantovani et al., 2001; Gelabert et al., 2001, 2002, 2004), back-arc extension helps to drive subduction. One of the possible reasons for such back-arc extension is compression parallel (or slightly oblique) to a continental margin. This might explain why some orogenic arcs start as straight features in plan view and then acquire curvature as their back-arc basins develop. Although a few physical experiments have tested this model (Faccenna el al., 1996), we know of none that have tested the relationship between back-arc extension and the density ratio between oceanic and continental plates. Therefore in this paper, we describe three series of experiments (32 in all), in which we tested the effects of (1) the density ratio between oceanic and continental plates and (2) shortening parallel to a continental margin.

Our experimental design follows that of Faccenna et al., (1996), who modelled the Tyrrhenian-Apennine system in a framework of collision between the African and Eurasian plates. Faccenna et al. (1996) in their experiments tested the influence of margin-parallel compression, but only within a continent. In contrast, we tested the effects of compression within oceanic and continental plates simultaneously, as well as the effects of a wider range of density ratios and velocities of plate convergence.

Finally, we have compared our experimental results with the history of back-arc extension in Anatolia.

2 Experimental Procedure

We did the experiments in the modelling laboratory at Géosciences Rennes (University of Rennes 1), using the experimental procedure of Davy and Cobbold (1988, 1991), which is based on simplified strength profiles of the lithosphere. For boundary conditions, we followed partially Becker et al. (1999).

The models simulated the formation of subduction zones and deformation at lithospheric scale. Each model consisted of one continental plate (CP) and one oceanic plate (OP). Between them was the continent-ocean boundary (COB).

2.1 Strength profiles

To calculate the vertical strength profile of the continental or oceanic lithosphere, we assume that the upper crust is brittle and that the lower crust is ductile. To model the mantle lithosphere, the number of layers should depend on the temperature: two-layer lithosphere for high temperatures; three-layer lithosphere for intermediate temperatures; four-layer lithosphere for low temperatures (Davy and Cobbold, 1991). For our purposes we assumed high temperature and therefore a two-layer lithosphere for Aegean system (see Gautier et al., 1999; Tesauro et al., 2009).

We consider that the oceanic lithosphere is a thermal boundary layer and its base is an isotherm. To calculate shapes of isotherms, we follow Turcotte and Schubert (1982). If the lithosphere cools in the same way as a semi-infinite half-space, a lithospheric segment that forms between 10 Ma and 35 Ma is up to 100 Km thick, moves at 3 cm/yr and, if the base of the lithosphere is at 1400º K, has an average slope of about 3^0. In our experiments, the base of the oceanic plate had a slope of 4^0.

2.2 Materials

Following previous authors (Faccenna et al., 1996, 1999, 2004, 2006; Becker et al., 1999; Regard et al., 2003, 2005, 2008) we used sand to model the brittle upper crust, silicone putty for the ductile lower crust (Tables 1 and 2) and honey for the asthenosphere.

The sand was a pure dry variety from Fontainebleau, France. This consists of more than 95% quartz. Grains are well-rounded and their size is between 2 x 10^{-4} and 4 x 10^{-4} m. The material yields according to a Mohr-Coulomb envelope, with negligible cohesion and an angle of internal friction between 30° and 40^0 (Krantz, 1991). The pure sand has a density of 1.56 g/cm³ (± 0.6 %) and this is what we used for the oceanic plate. In contrast, for the continental plate the density was 1.36 g/cm³ (± 1.5 %), because we mixed the sand with ethyl-cellulose powder. This did not change the mechanical properties of the sand. We measured the density of the sand by first sieving it into a dish of known volume and then recording its weight. This we did 3 times, so as to obtain an average value.

The pink silicone putty (Silbione Gomme 70009, Rhône Poulenc, France) is a Newtonian fluid, in other words, it has a linear dependence of strain rate upon stress. At room temperature (20 ± 2^{0}C), the density of the pure silicone is about 1.2 g/cm³ and the viscosity is about 10^4 Pa s. The viscosity varies with temperature (Weijermars, 1986). To investigate the effects of various densities in the models, we mixed the silicone with heavy mineral powders, so that the density of the mixture for the continental plate was between 1.175 and 1.346 g/cm³ and the viscosity was between 31700 and 56800 Pa s

(± 10 %). For the oceanic plate, the density of the silicone was between 1.33 and 1.67 g/cm³ (± 1 %), and the viscosity was between 26800 and 153000 Pa s. To measure the density, we first weighed a sample of silicone and then dropped it into water, to record the increase in volume. This we did 3 times, so obtaining an average value. To measure the viscosity and check the flow law, we used a thick-ring rotary viscosimeter, of the kind that was in use at Uppsala University in 1981 (see Weijermars, 1986; Cobbold and Jackson, 1992). In such a viscometer, both the stress and the flow rate vary radially, allowing the operator to obtain a flow law, by observing the change in shape of a radial line on the free surface. The precision of this method is ± 5% and we repeated all measurements 3 times to decrease errors.

The density of the natural honey that represented the asthenosphere was 1.43 g/cm³ and the viscosity was 10^2 Pa s. We measured and carefully controlled these values. We obtained the viscosity and the flow law from a thick-ring rotary viscometer, as well as by dropping spherical objects into a column of honey and using Stokes' Law (Lamb, 1994).

2.3 Scaling

We adopted the experimental procedure of Davy and Cobbold (1988, 1991) for lithospheric modelling (see Table 2 for the parameters and model ratios). The length ratio was 3×10^6 (1 cm representing 30 km in nature). The density ratio was between 2 and 2.5, therefore, according to Davy and Cobbold (1991), the stress ratio was about 8×10^6, and the time ratio was 6×10^9.

In nature, the density of oceanic lithosphere varies, but in our models we did not take this into account. Instead, we used a silicone layer of uniform density, but variable thickness, having an average basal slope of 4°.

2.4 Apparatus and procedure

Each model consisted of two plates, an oceanic plate (in blue, Fig. 1) and a continental plate (in dark grey).

We built and deformed all models inside a rectangular tank (40 × 40 cm, corresponding to 1200 × 1200 km in Nature; Table 1). The base and walls of the tank were of rigid transparent material. The models were built up layer by layer.

To deform the models, we used two kinds of pistons (Fig. 1). In experiments of Series A, the piston was as wide as the model (40 cm), its leading edge was in contact with the oceanic plate and it advanced in a direction perpendicular to the COB. In experiments of Series B, the piston was also wide (40 cm), but its leading edge was perpendicular to the COB and it advanced in a direction parallel to the COB, compressing both the oceanic and continental plates. Finally, in experiments of Series C, the piston was narrower (20 cm), so that its leading edge spanned the continental pate. As in Series B, the piston was perpendicular to the COB and it advanced in a direction parallel to the COB. However, it compressed the continental plate only.

To record progressive deformation at the surface of the model, we laid down a grid of thin white lines of sand at a spacing of 5 cm and photographed it every 15 minutes. We

also took photographs of the lateral boundaries of the model, visible through the transparent sidewalls.

To measure the amount of extension, we calculated local changes in surface area of the continental and oceanic plate, by counting pixels automatically on the photographs. This procedure yields the percentage areas of piston, continental plate and oceanic plate. Each of these values changed with time, the area of the piston varying at the same rate in all the experiments having the same piston size (see Fig. 6a, b, c, for Series A).

In our experiments, we did not investigate the possible effects of other parameters, such as (1) the viscosity and flexural resistance of the oceanic plate (Becker et al., 1999; Regard et al., 2003; Funiciello et al., 2008), (2) conditions at the base of a subducting slab (Regard et al., 2003; Guillaume et al., 2009), (3) slab break-off (Regard et al., 2008; Regard et al., 2003), (4) relative thicknesses of oceanic and continental plates (Faccenna et al., 1999; Nikolaeva et al., 2010), or (5) free lateral boundaries of subducting plates (Funiciello et al., 2004).

3 Experimental results

Of the three series of experiments, those of Series A were to determine which was the most appropriate piston velocity, whereas those of Series B and C were to investigate the influence of the density contrast, for two different widths of piston.

To simplify the description (Figs. 2 to 5), we will use geographical coordinates, such that North is upwards and the piston is in the West. This means that the displacement of the piston is always eastwards.

Following previous workers (e.g. Faccenna et al., 1996, 1999, 2003, 2006; Becker et al., 1999; Regard et al., 2005, 2008), we used a rectangular box, which had rigid lateral boundaries. Inevitably, these led to some boundary effects, resulting from rigidity and from sidewall friction. In our experiments, the effects of friction were visible over a distance of 2 to 3 cm from the sidewalls. However, we realize that their mechanical effects may have extended further across the model, and they might have contributed to increase normal faulting near the north-eastern corner.

When continental material was spreading over the oceanic plate, the deformation affected the entire continental plate (sand and silicone).

We stopped the piston after 12 hours in almost all the experiments. For a piston moving at 0.5 cm/h, 12 hours corresponded to 6 cm of shortening, in other words, 120 km in nature, which is a reasonable value.

3.1 Series A

In experiments of Series A, the piston was as wide as the model (40 cm), its leading edge was in contact with the oceanic plate and it advanced in a direction perpendicular to the COB. The piston velocities were 0.1, 0.5 or 2.5 cm/h. Surface views before deformation show an initially linear COB (Fig. 2, Series A). The total displacement was 2.4 cm for model A1 and 6 cm for models A2 and A3.

In Model A1 the velocity was 0.1 cm/h. Extension initiated in the continental plate, next to the COB, and propagated westward toward the piston. After 20 hours (2 cm of piston displacement), the oceanic plate had subducted almost completely, while the continental plate had extended from 20 cm to about 35 cm. After 24 hours (2.4 cm of piston displacement), there was no further change and we stopped the experiment.

In Model A2 the velocity was 0.5 cm/h. Folding of the oceanic plate started after 2 hours (1 cm of piston displacement); subduction of the oceanic plate, after 4 hours (2 cm of piston displacement); and extension of the continental plate, after 7 hours (3.5 cm of piston displacement). At the end of the experiment, after 12 hours (6 cm of displacement), a zone in the continental plate near the COB was still undergoing extension, while the oceanic plate was shortening and subducting.

In Model A3 the velocity was 2.5 cm/h. Folding of the oceanic plate started after 0.5 hours (1.25 cm of piston displacement); subduction of the oceanic plate, after 1 hour (2.5 cm of piston displacement); but no extension was visible in the continental plate. When the piston stopped, after 2.4 hours (6 cm of piston displacement), the oceanic plate was still shortening and subducting.

In both models A1 and A2, extension of the continental plate and shortening of the oceanic plate occurred synchronously. However in model A2 displacement of the piston was balanced by shortening and subduction of the oceanic plate with minor deformation of the continental plate. Thus, after this first series of experiments, using different velocities, we decided to adopt a piston velocity of 0.5 cm/h (Fig. 2), corresponding to

1.5 cm/yr in nature (Table 2). In the future it might be interesting to test other velocities and to compare the results.

3.2 Series B

For this series, we again used a wide piston (40 cm), which moved eastwards, perpendicularly to the COB (Figs. 2 and 3). In the early stages (0 to 12 hours) the piston moved at a steady velocity of 0.5 cm/h, whereas in later stages (12 to 18 hours) it was stationary. Before deformation, the COB was straight (Fig. 2, Series B).

We will describe six stages in the development of Model 7 (after 3, 6, 9, 12, 15 and 18 hours, Fig. 3).

Stage 1 (3 hours). By this stage, the COB, especially its western part, had moved southwards. Slight bending, next to the piston and opposite sidewall, was a boundary effect, due to friction, and was also visible at later stages. In the south-western part of the continental plate, where the displacement of the COB was larger, elements of the reference grid had become somewhat rectangular, so that the total area of the continental plate had increased by about 2.7%. In the north-western part of the oceanic plate, near the COB, E-W-trending folds (fo1) and reverse faults had appeared. Elsewhere in the oceanic plate, the square grid had not deformed.

Stage 2 (6 hours). By this stage, the COB had rotated counter-clockwise and its western part had moved further southward. At 21.5 cm from the piston, a slight change in strike defined an inflexion point (Inf). More generally, offsets of the grid lines demonstrated a small amount of right-lateral shear along the COB. In the continental

plate, North-trending folds (fc1) appeared near the piston in the north-western corner of the model. Also, several major right-lateral faults (d) and minor conjugate left-lateral faults appeared in the south-western and central area of the continental plate. At the end of one right-lateral fault, a zone of extension (e1) developed. In western areas (at 5 to 15 cm from the piston), where the displacement of the COB was larger, elements of the reference grid had become more rectangular and, next to the COB, the sand layer had thinned and faulting was diffuse. At this stage, the total area of the continental plate had increased by about 2.4% since the start of the experiment, but had decreased by 0.2% since Stage 1. In the oceanic plate, new North-trending folds (fo2) had appeared near the piston in the western area. Elsewhere in the oceanic plate, the square grid showed little or no deformation.

Stage 3 (9 hours). By this stage, southward displacement of the COB had increased. The inflexion point (Inf) had migrated eastward through the material, remaining at 21.5 cm from the piston. Right-lateral slip along the COB had increased. In the continental plate, new North-trending folds formed in the north-western corner of the model (fc1) and more centrally (fc2). Strike-slip faults formed a triangular pattern, with a new major left-lateral fault (s) in the North and right-lateral fault (d) in the South. At the eastern ends of these faults, in the centre of the continental plate, the original zone of extension (e1) had become more visible, while a new one (e2) had developed further north. Where the displacement of the COB was larger, near the piston, the zone of diffuse faulting had become wider. The greatest distortion of the surface grid was in an area about 5 to 15 cm in front of the piston. To a first approximation, elements of the grid had rotated about

6º clockwise in the south-western area and 11º counter-clockwise in the south-central area. At this stage, the total area of the continental plate had increased by about 5.9% since the start of the experiment, and by 3.4% since Stage 2. In the oceanic plate, the North-trending folds (fo2) had propagated to the South, while the COB had overridden them in the North. Where the displacement of the COB was larger, a sharp fold (dashed line) appeared within the oceanic plate, parallel to the COB. Elsewhere in the oceanic plate, the square grid showed little or no deformation.

Stage 4 (12 hours). At this stage we stopped the advance of the piston. Southward displacement of the COB had increased even more. The inflexion point was at 23 cm beyond the piston. Right-lateral slip along the COB reached a maximum at a point between 12 and 20 cm in front of the piston. In the continental plate, some of the folds, which had formed at Stage 3, were still active. The left-lateral fault (s) had lengthened and the right-lateral fault (d) had shortened. The previous zones of extension (e1 and e2) had become even more visible, while another one (e3) had appeared further South. Where the displacement of the COB was greater, in the western area, the zone of diffuse faulting had enlarged. The greatest distortion of the surface grid was in an area about 5 to 17 cm in front of the piston. To a first approximation, elements of the grid had rotated about 14^0 clockwise in the south-western area (8^0 since Stage 3), and 22^0 counter-clockwise in the south-central area (11^0 since Stage 3). At this stage, the total area of the continental plate had increased by about 8.8% (2.9% since Stage 3). In the oceanic plate a new North-trending fold (fo3) had formed in front of the southern area of maximum curvature of the COB, the previous fold (fo2) had developed further, while the

COB had overridden it in the North. Apart from the sharp fold (dashed line) within the oceanic plate, the square grid showed little or no deformation.

Stage 5 (15 hours). By this stage the piston was stationary. Southward displacement of the COB had increased even more. The inflexion point was still at 23 cm beyond the piston. Left-lateral slip had occurred along the first 4 cm of the COB in front of the piston and right-lateral slip was present further away. In the continental plate the left-lateral fault (s) had lengthened and almost traversed the model, from the piston to the opposite wall. The previous zones of extension (e1, e2 and e3) had increased, while another small one had appeared (next to e2). Where the displacement of the COB was greater, in the western area, the zone of diffuse faulting had enlarged. The greatest distortion of the surface grid was within 23 cm of the piston. Elements of the grid had rotated, by about 25^0 counter-clockwise in the south-central area (3^0 since Stage 4). At this stage, the total area of the continental plate had increased by about 17.9% (9.1% since Stage 4). Apart from the sharp fold (dashed line) within the oceanic plate, the square grid showed little or no deformation.

Stage 6 (18 hours). By this stage the piston was stationary. Southward displacement of the COB had increased even more. The inflexion point was still at 23 cm beyond the piston. Left-lateral slip had occurred along the first 4 cm of the COB in front of the piston and right-lateral slip was present further away. In the continental plate, the left-lateral fault zone (s) had widened and shortened (the fault had an extensional component). Right-lateral faults (d in the previous stage) had vanished. The previous zones of extension (e1, e2 and e3) had increased in area. Where the displacement of the COB

was greater, in the west-central area, the zone of diffuse faulting had enlarged. The greatest distortion of the surface grid was within 26 cm of the piston. Elements of the grid had rotated about 29^0 counter-clockwise in the south-central area (4^0 since Stage 5). At this stage, the total area of the continental plate had increased by about 26.3% (8.4% since Stage 3). In the oceanic plate a new East-trending fold (fo4) had formed to the SE of the COB. Apart from the sharp fold (dashed line) within the oceanic plate, the square grid showed little or no deformation.

3.3 Series C

For this series, we used a narrow piston (20 cm), which moved eastwards, perpendicularly to the COB (Figs. 2 and 4). In the early stages (0 to 12 hours) the piston moved at a steady velocity of 0.5 cm/h, whereas in later stages (12 to 18 hours) it was stationary. Before deformation, the COB was straight (Fig. 2, Series C), after shortening the asymmetric curvature of the COB may be due to the size of the piston.

We will describe 6 stages in the development of Model 8 (after 3, 6, 9, 12, 15 and 18 hours, Fig. 4).

Stage 1 (3 hours). By this stage, the COB, especially its western part, had moved southwards. Slight bending, next to the piston and to the opposite sidewall, was probably due to friction. These boundary effects were visible also at later stages. At 23 cm from the piston, a slight change in strike defined an inflexion point (Inf). Left-lateral slip had occurred along the first 12 cm of the COB in front of the piston and right-lateral slip was present further away. In the continental plate, two elongate extension zones (e_1

and e2) developed parallel to the COB, in northern and central areas. At the eastern end of the extension zones, we observed left-lateral faults (s) striking NW-SE. In western areas, where the displacement of the COB was larger, elements of the reference grid next to the COB had become somewhat rectangular, the sand layer had thinned and faulting was diffuse. In the eastern area, where the displacement of the COB was smaller, a group of small normal faults had appeared, striking NW-SE. At this stage, the total area of the continental plate had increased by about 13.3%. Elsewhere in the oceanic plate, the square grid had not deformed.

Stage 2 (6 hours). By this stage, southward displacement of the COB had increased and had become symmetric. Left-lateral slip had increased along the first 12 cm of the COB in front of the piston and right-lateral slip was present further away. In the continental plate, the extension zones (e1 and e2) had propagated and branched out sideways. At the eastern end of these extension zones, left-lateral faults were still active. In front of the piston, strike-slip faults formed a triangular pattern, with a new left-lateral fault (s) in the North and a right-lateral fault (d) in the South. Normal faults appeared, next to the area of diffuse faulting, and propagated in a direction almost perpendicular to the COB. The zone of diffuse faulting had become wider, forming a belt across the continental plate, north of the COB. The greatest distortion of the surface grid was in an area about 10 to 20 cm in front of the piston. To a first approximation, elements of the grid had rotated about 19^0 clockwise in the south-western area and 17^0 counter-clockwise in the south-central area. At this stage, the total area of the continental plate had increased by about 30.6% since the start of the experiment (17.3% since Stage 1).

In the oceanic plate, where the displacement of the COB was larger, a sharp fold (dashed line) had appeared within the oceanic plate, parallel to the COB. Elsewhere in the oceanic plate, the square grid showed little or no deformation.

Stage 3 (9 hours). By this stage, southward displacement of the COB had increased. Left-lateral slip had increased along the first 15 cm of the COB in front of the piston and right-lateral slip was present further away. In the continental plate, the extension zones (e1 and e2) had become larger. In front of the piston, strike-slip faults still formed a triangular pattern, with a left-lateral fault (s) in the North and a right-lateral fault (d) in the South. New normal faults appeared, next to the area of diffuse faulting, and propagated in a direction almost perpendicular to the COB. The zone of diffuse faulting, north of the COB, had become narrower. To a first approximation, elements of the grid had rotated about 30^0 clockwise in the south-western area and 25^0 counter-clockwise rotation in the south-central area. At this stage, the total area of the continental plate had increased by about 39.8% since the start of the experiment (9.2% since Stage 2). Apart from the sharp fold (dashed line) next to the COB, the square grid showed little or no deformation in the oceanic plate.

Stage 4 (12 hours). At this stage we stopped the advance of the piston. Southward displacement of the COB had increased. Left-lateral slip had increased along the first 15 cm of the COB, in front of the piston, and right-lateral slip was present further away. In the continental plate, the extension zones (e1 and e2) had propagated further, surrounding rigid blocks, which had moved towards the oceanic plate. In front of the piston, left-lateral faults (s) were still active. The normal faults, which had formed roughly

perpendicular to the COB, had become wider and somewhat longer. The zone of diffuse faulting had become narrower. To a first approximation, elements of the grid had rotated about 39^0 clockwise in the south-western area and 38^0 counter-clockwise in the south-central area. At this stage, the total area of the continental plate had increased by about 49% since the start of the experiment (9.2% since Stage 3). Apart from the sharp fold (dashed line) next to the COB, the square grid showed little or no deformation in the oceanic plate.

Stage 5 (15 hours). By this stage the piston was stationary. Southward displacement of the COB had increased even more. Left-lateral slip had increased along the first 16 cm of the COB in front of the piston and right-lateral slip was present further away. In the continental plate, the extension zones had become larger, isolating more blocks. Left-lateral faults (s) were still active. The normal faults, which had formed roughly perpendicular to the COB, had become wider and longer, isolating a few blocks. The zone of diffuse faulting had become narrower. To a first approximation, elements of the grid had rotated about 48^0 clockwise in the south-western area and 49^0 counter-clockwise in the south-central area. At this stage, the total area of the continental plate had increased by about 52.9% since the start of the experiment (3.9% since Stage 4). In the oceanic plate, where the displacement of the COB was larger, a sharp fold (dashed line) appeared within the oceanic plate, parallel to the COB. Elsewhere, the square grid showed little or no deformation in the oceanic plate.

Stage 6 (18 hours). By this stage the piston was stationary. Southward displacement of the COB had increased even more. Left-lateral slip had increased along the first 17.5 cm

of the COB, in front of the piston, and right-lateral slip was present further away. In the continental plate, the extension zones had become larger, isolating more blocks. The zone of diffuse faulting in central areas had become so narrow, that continental blocks had reached the COB. To a first approximation, elements of the grid had rotated about 50^0 clockwise in the south-western area and 52^0 counter-clockwise rotation in the south-central area. At this stage, the total area of the continental plate had increased by about 67.8% since the start of the experiment (14.9% since Stage 5). Apart from the sharp fold (dashed line) next to the COB, the square grid showed little or no deformation in the oceanic plate.

3.4 Experiments of Series B and Series C for various density ratios

We will now describe experiments of Series B and C (small or large piston) after 12 hours (6 cm of displacement), when the piston had stopped moving, and for various values of the density ratio ($R = \rho_o/\rho_c$), where ρ_o is the density of the oceanic plate and ρ_c is the density of the continental plate (Fig. 5).

Density ratio: 1.13 - 1.16

Model 5, Series B. For this density ratio (1.13 - 1.16), the pattern of grid lines at the COB showed bilateral symmetry, but little deformation. Offsets of the grid lines demonstrated a small amount of right-lateral shear along the eastern part of the COB. In the continental plate, North- and Northwest-trending folds developed on the western side of the model, near the piston. Strike-slip faults formed a triangular pattern, with a major left-lateral fault in the North and a right-lateral fault in the South. Another left-lateral slip fault

formed at the northern boundary of the model. In the north-eastern part of the model, an extension zone developed. No zone of diffuse faulting was visible. In the oceanic plate, North-trending folds formed in three places: (1) in the western area, next to the piston, (2) in the centre, where the curvature of the COB was a maximum, and (3) in the eastern area, next to the sidewall. Furthermore, East-trending folds appeared in the southern area.

Model 4, Series C. For this density ratio (1.13 - 1.16), the pattern of grid lines at the COB showed very little deformation. Offsets of the grid lines demonstrated a small amount of right-lateral shear along the COB. In the continental plate, Northwest-trending folds formed in the northern area of the model and North-trending folds in the south-eastern area. A major Northwest-trending left-lateral fault formed between these two fold families. No zone of diffuse faulting was visible. At the northern edge of the oceanic plate, near the COB, E-W-trending folds appeared.

Density ratio: 1.33 - 1.34

Model 7, Series B. For this density ratio (1.33 - 1.34), the COB bulged southwards as far as the inflexion point. Right-lateral slip occurred along the COB. In the continental plate, North-trending folds appeared in the north-western area and major strike-slip faults crosscut the plate, forming a zone of extension where they intersected. A zone of diffuse faulting appeared, where the displacement of the COB was greater. In the oceanic plate, a North-trending fold formed next to the COB and a sharp fold (dashed line) developed parallel to the COB, where its displacement was larger.

Model 6, Series C. For this density ratio (1.33 - 1.34), the COB bulged symmetrically southward. Slip was left-lateral along the western part of the COB and right-lateral along its eastern part. In the continental plate, there was a large area of diffuse faulting, where a series of minor left-lateral faults were visible. Where the displacement of the COB was larger, a sharp fold (dashed line) appeared within the oceanic plate, parallel to the COB.

Density ratio: 1.41 - 1.42

Model 9, Series B. For this density ratio (1.41 - 1.42), the COB underwent a large southward displacement. Right-lateral slip occurred along the COB. In the continental plate, extension zones linked, isolating rigid blocks, which also moved southwards, rotating clockwise in the south-western area and counter-clockwise in the south-central area. In the North, left-lateral faults were active. The zone of diffuse faulting formed a long narrow belt next to the COB. In the oceanic plate, where the displacement of the COB was larger, a sharp fold (dashed line) appeared within the oceanic plate, parallel to the COB.

Model 8, Series C. For this density ratio (1.41 - 1.42), the COB underwent a large southward displacement. Left-lateral slip occurred along the western part of the COB and right-lateral slip along its eastern part. In the continental plate, extension zones linked, isolating rigid blocks, which moved southwards, rotating clockwise in the south-western area and counter-clockwise in the south-central area. In the North, left-lateral faults were active. The zone of diffuse faulting formed a long narrow belt next to the COB. In the oceanic plate, where the displacement of the COB was larger, a sharp fold (dashed line) appeared within the oceanic plate, parallel to the COB.

4 Discussion

Effect of density contrast

In a first group of experiments (Model 5 of Series B and Model 4 of Series C), where the density ratio (between oceanic and continental plate) was 1.1, the percentage area of continental plate changed very little, while the piston was in motion. Until the end of each experiment (percentage area of 2.2 % for a wide piston and -2.2% for a narrow piston, after 18 hours) there was no extension and no oceanic subduction (Fig. 6a).

In a second group of experiments (Model 7 of Series B and Model 6 of Series C), where the density ratio was 1.3, the percentage area of continental plate changed little (8.7% for a wide piston and 20.8% for a narrow piston), while the piston was moving, but changed much more (17.4% for a wide piston and 32.3% for a narrow piston) after the piston had stopped (after 12 hours) and until the end of observations (18 hours for series B and 15 hours for series C). After 6h of compression, the oceanic plate started to subduct; the slab sank slowly, while the piston was in motion, but much more quickly, after the piston had stopped (Fig. 6b).

In a third group of experiments (Model 9 of Series B and Model 8 of Series C), where the density ratio was 1.4, the percentage area of continental plate increased steadily from the beginning to the end of the experiment (by 42.8% for a wide piston and by 67.8% for a narrow piston, after 18 hours). After 3h of compression, the oceanic plate started to subduct; the slab then sank continuously and fast (Fig. 6c). However, the surface area

increased to higher values for the narrow piston than it did for the wide piston. A narrow piston provided more space for a continental plate to spread over the adjacent oceanic plate.

For all these experimental results (Series B and C), we infer that the density ratio (between oceanic and continental plates) was a very important factor in facilitating extension in the continental plate during subduction (Fig. 7). When the density ratio was lower than 1.2-1.25, no extension occurred in the continental plate. When the density ratio was between 1.25-1.35, extension occurred in the continental plate, although mainly after compression stopped. Finally, when the density ratio was higher than 1.35, extension occurred in the continental plate from the very beginning of the experiment.

Most authors have assumed that an oceanic plate is denser than the underlying asthenosphere and some have investigated the effect of systematically varying the density ratio between the two, either in physical models (Faccenna et al., 1999; Shemenda, 1994) or in numerical models (Becker et al., 1999; Nikolaeva et al., 2010). When other parameters remained constant, the rate of subduction was higher for larger density ratios and we agree with that conclusion.

The dimensionless buoyancy number, F (Houseman and Gubbins, 1997; Faccenna et al., 1999) is a measure of the density contrast between oceanic lithosphere and asthenosphere, as well as the thickness and ductile resistance of the oceanic lithosphere:

$$F = L^2 \, g \, \Delta\rho / u \, \eta \qquad (1)$$

Here L is the thickness of the oceanic plate (h sand + h silicone), η is the viscosity (of what) (which we have denoted as μ), u is the velocity of convergence of the piston, g is the gravitational acceleration, and $\Delta\rho$ is the density contrast between the oceanic lithosphere and the asthenosphere.

We have calculated the buoyancy number for all of our experiments (Table 1). For the second and third group of experiments, F>1 and we observed subduction, whereas for model 5 of the first group of experiments, F<1 and there was no subduction. These results are in agreement with the observations of Faccenna et al. (1999). In contrast, for Model 4, F>1, yet there was no subduction. We infer that, although the buoyancy number is important in determining if subduction will occur, it is not the only factor. We suggest that the density ratio between oceanic and continental plates is also important. In our experiments, subduction did not occur, even for F>1, if the density ratio was not high enough (Table 1 and Fig. 7).

Piston velocity

In previous experimental studies, as in our own, it is clear that piston velocity was one of the most important parameters controlling subduction and continental extension (Faccenna et al., 1996; Becker et al., 1999). When the piston velocity was fast, no extension was visible in the continental plate. In contrast, when the velocity was slow, extension of the continental plate and subduction of the oceanic plate occurred synchronously. However, these two processes did not always balance, so that in some experiments there was much extension, for almost no piston displacement (Fig. 2).

Having said this, we would like to make it clear that, in our experiments, the following parameters were equally important, if not more so, in controlling the amount of continental extension.

Convergence history

Although some authors have described what happened when a converging piston stopped moving (Faccenna et al., 1996, 1999; Becker et al., 1999), we have investigated this more fully. For various density ratios between continental and oceanic plates, we found that extension continued to accumulate, even after the piston stopped (Fig. 6). Moreover we found that the density ratio between continental and oceanic plates had important effects on the styles of subduction and continental extension, for all directions of piston convergence.

Viscosity and flexural resistance of the oceanic plate, slab break-off

Previous authors (Becker 1999; Regard et al., 2003, 2005, 2008; Funiciello et al., 2008) have concluded that the rheological properties of the slab are important, in that they control the development of the subduction zone. According to Regard et al. (2008), viscous removal of the denser parts of the slab decreases the slab-pull force. However, if the slab is strong, it does not deform and the slab-pull force remains active. The other way for a slab to deform is by breaking off entirely. Pyskywec et al. (2000) have modelled this process numerically.

Conditions at the base of a subducting slab

In all experiments, the thickness of the lowermost ductile layer influences the development of viscous instabilities (Regard et al., 2003). A very thick layer favours the formation of instabilities, but we did not study this parameter. In all our models the initial thickness of honey was the same.

5 Comparing models and nature

The Aegean-Anatolian orocline and back-arc system have developed in a context of convergence of the African plate with Eurasia since the Upper Jurassic (Sengör and Yilmaz, 1981; Robertson and Dixon, 1984). The present-day Aegean-Anatolian system is bounded to the north by the right-lateral North Anatolian Fault (NAF), to the east by the left-lateral East Anatolian Fault (EAF) and to the south by the Hellenic and Cyprus Subduction Zones (Fig. 8).

Although both the Hellenic Subduction Zone and the Cyprus Subduction Zone have accommodated large amounts of plate convergence between Africa and Eurasia, the former has a back-arc area where extension is large - the Aegean Sea - whereas the latter has a back-arc area - Central Anatolia - where extension is small.

The back-arc area of the Hellenic Subduction Zone, North of Crete, includes the Aegean Sea and surrounding areas. Late Cenozoic extension has been responsible for exhumation of several metamorphic complexes (Cyclades, Menderez and at least some part of Rhodope) (Lister et al., 1984; Gautier at el., 1999 and Jolivet et al., 2012). Extension in a roughly NNE-SSW direction occurred by southward retreat of the Hellenic

trench (Mercier et al., 1989; Le Pichon and Angelier, 1981; Gautier at al., 1999 and Van Hinsberger and Schmid, 2012). This was coeval with southward migration of magmatism, from the Rhodope Massif to the Cyclades (since about 35 Ma according to Jolivet et al., 2013).

The back-arc area of the Cyprus Subduction Zone, north of Cyprus, includes the region of Central and East Anatolia, a Mesozoic to Tertiary collision zone. This region consists of three main terrains with ophiolitic sutures. These terrains are, from north to south, the Pontides, Central Anatolian Crystalline Complex and Taurides (Moix et al., 2008). The Central Anatolian Crystalline Complex consists of high-grade metamorphic rocks intruded by late granitoids (Floyd et al., 2000). This complex was formerly covered by ophiolitic nappes, which are now widespread in the Anatolian terrains (Moix et al., 2008). For this region, South of the North Anatolian Fault, the tectonic setting during the Cenozoic is debatable. It could be a strike-slip system (Koçyigit and Beyham 1998) a compressional system (Gülyüz et al., in press) or an extensional system (Genç and Yürür, 2010). In any case, unlike in the Aegean area, there has not been so much extension as to produce a metamorphic core complex (see discussion in Gautier et al., 2002).

The question is: why, in one geodynamic setting, are the tectonic responses so different? According to Jolivet et al. (2013), extension in the Aegean began at 35 Ma or before. In contrast, westward extrusion of Anatolia may not have started before 10-13 Ma (Sengör et al., 1985). Therefore lateral shortening may have helped to control subduction and continental extension only during the later stages.

A map of Bouguer gravity anomalies for Turkey shows a residual positive anomaly in Central Anatolia (Ates et al., 1999), which could be due to the high density of deep crustal rocks. In contrast, the rocks forming the Aegean Sea are mainly sedimentary or metasedimentary, so of low density. Exceptions are metamorphic rocks in the Cyclades, Menderez and the Rhodope Metamorphic Complex, of which the exhumation partly resulted from Aegean extension. Thus, prior to the extension, the density of the continental lithosphere could have been higher, north of the Cyprus Subduction Zone, than it was north of the Hellenic Subduction Zone. If so, and if the oceanic lithosphere had the same density south of both subduction zones, the density ratio between the oceanic and continental lithospheres was higher, across the Hellenic subduction zone, than it was across the Cyprus subduction zone. We suggest that a high density ratio has been an important driving force for Aegean extension, while in Central Anatolia a low density ratio may have prevented extension. Likewise in our models, density ratio has been a key factor.

In general, three other factors may influence the lithospheric density variations between subducting lithosphere and continental lithosphere in order to favour back-arc extension.

1) Initial properties of the oceanic plate. Variations in the properties of the subducting lithosphere (more oceanic versus less oceanic) may explain the difference in resulting back-arc extension. A more oceanic composition means that the density is higher, so that the density ratio between subducting lithosphere and continental lithosphere is higher, so favouring back-arc extension.

2) Hydration of the lithospheric upper plate. During subduction processes, dehydration of the downgoing plate (Peacock, 1993; Ringwood 1974) causes hydration of the upper mantle wedge (Hyndman et al., 2003; Arcay et al., 2005). This will change its physical properties, including density and seismic velocity (Bostock et al., 2002; Hacker et al 2003). A decrease in density of the upper plate, due to hydration of the mantle wedge, may contribute to back-arc extension (Arcay et al., 2005; Levander et al., 2011)

3) Initial continental thickness. The initial crustal thickness could have been large enough to favour gravity spreading.

6 Conclusions

For the experiments, we draw the following conclusions.

- In every experiment, where there was extension in the continental plate, there was also subduction of the oceanic plate.

- However, in some experiments, there was subduction of the oceanic plate, but no extension in the continental plate. Therefore subduction was not enough to explain continental extension.

- Compression parallel to the continent-ocean boundary did not favour continental extension.

- In contrast, the density ratio between the oceanic plate and continental plate was a key factor: the higher the density ratio, the greater the amount of extension in the continental plate during subduction.

For the application to Anatolia, we draw the following conclusions.

- Despite similar geological settings, the areas north of the Hellenic and Cyprus subduction zones differ, in that extension is larger in the former and much smaller in the latter.

- In the light of our experiments, an important control on extension and retreat of the trench should be the density ratio between oceanic and continental plates. Accordingly, we suggest that Aegean extension was due to a high density ratio between subducting oceanic lithosphere and a Hellenic-Balkanic upper plate of relatively low density, whereas in the Anatolian upper plate (of relatively high density) the density contrast was lower and there was less extension.

Acknowledgements:

The authors would like to thank J.-J. Kermarrec for his valuable technical assistance. This work was part of the Spanish Research Project, "El significado del Promontorio Balear" (CGL2008-05724BTE), which provided funding. Drs. Pierre Gautier and Romain Bousquet provided valuable comments on the tectonic context of Anatolia. We thank Reviewers 1 and 3 for their very detailed reviews and constructive suggestions that helped us to improve the manuscript.

References

Arcay, D., Tric E., Doin, M.-P., 2005. Numerical simulations of subduction zones: Effect of slab dehydration on the mantle wedge dynamics. Physics of the Earth and Planetary Interiors 149, 133-153.

Ates, A., Kearey, P., Tufan, S., 1999. New gravity and magnetic anomaly maps of Turkey. Geophysical Journal International 136, 499-502.

Becker, T.W., Faccenna, C., O'Connell, R.J., Giardini, D., 1999. The development of slabs in the upper mantle: Insights from numerical and laboratory experiments. Journal of Geophysical Research: Solid Earth 104, 15207-15226.

Bostock, M.G., Hyndman, R.D., Rondenay, S., Peacock, S.M., 2002. An inverted continental Moho and the serpentinization of the forearc mantle. Nature 417, 536-538.

Chemenda, A.I., Hurpin, D., Tang, J.-C., Stephan, J.-F., Buffet, G., 2001. Impact of arc-continent collision on the conditions of burial and exhumation of UHP/LT rocks: experimental and numerical modelling. Tectonophysics 342, 137-161.

Cobbold, P.R., Jackson, M.P.A., 1992. Gum rosin (colophony): A suitable material for thermomechanical modelling of the lithosphere. Tectonophysics 210, 255-271.

Davy, Ph., Cobbold, P.R., 1991. Experiments on shortening of a 4-layer model of the continental lithosphere. Tectonophysics 188, 1-25.

Davy, P., Cobbold, P.R., 1988. Indentation tectonics in nature and experiment. 1. Experiments scaled for gravity. Bulletin of the Geological Institutions of Uppsala, New Series 14, 129-141.

Dewey, J.F., 1980. Episodicity, sequence and style at convergent plate boundaries. In: D.W. Strangway (Ed.), The Continental Crust and its Mineral Deposits, Geological Society of Canada Special Volume 20, 553-573.

Faccenna, C., Giardini, D., Davy, P., Argentieri, A., 1999. Initiation of subduction at Atlantic-type margins: Insights from laboratory experiments. Journal of Geophysical Research: Solid Earth 104, 2749-2766.

Faccenna, C., Bellier, O., Martinod, J., Piromallo, C., Regard, V., 2006. Slab detachment beneath eastern Anatolia: A possible cause for the formation of the North Anatolian fault. Earth and Planetary Science Letters 242, 85–97.

Faccenna, C., Piromallo, C., Crespo-Blanc, A., Jolivet, L., Rossetti, F., 2004. Lateral slab deformation and the origin of the western Mediterranean arcs. Tectonics 23, TC1012, doi:10.1029/2002TC001488.

Faccenna, C., Davy, P., Brun, J.-P., Funiciello, R., Giardini, D., Mattei, M., Nalpas, T., 1996. The dynamics of back-arc extension: an experimental approach to the opening of the Tyrrhenian Sea. Geophysical Journal International 126, 781-795.

Floyd, P.A., Göncüoğlu, M.C., Winchester, J.A., Yaliniz, M.K., 2000. Geochemical character and tectonic environment of Neotethyan ophiolitic fragments and metabasites

in the Central Anatolian Crystalline Complex, Turkey. Geological Society, London, Special Publications 173, 183-202.

Funiciello, F., Faccenna, C., Giardini, D., 2004. Role of lateral mantle flow in the evolution of subduction systems: insights from laboratory experiments. Geophysical Journal International 157, 1393-1406.

Funiciello, F., Faccenna, C., Heuret, A., Lallemand, S., Di Giuseppe, E., Becker, T.W., 2008. Trench migration, net rotation and slab-mantle coupling. Earth and Planetary Science Letters 271, 233-240.

Gautier, P., Brun, J.-P., Moriceau, R., Sokoutis, D., Martinod, J., Jolivet, L., 1999. Timing, kinematics and cause of Aegean extension: a scenario based on a comparison with simple analogue experiments. Tectonophysics 315, 31-72.

Gautier, P., Bozkurt, E., Hallot, E., Dirik, K., 2002. Dating the exhumation of a metamorphic dome: geological evidence for pre-Eocene unroofing of the Niğde Massif (Central Anatolia, Turkey). Geological Magazine 139, 559-576.

Gelabert Ferrer, B., Sàbat i Montserrat, F., Rodríguez-Perea, A., Fornós, J.J., 2004. On the origin of the North Pacific arcs. Geologica Acta 2, 203-212.

Gelabert, B., Sàbat, F., Rodríguez-Perea, A., 2002. A new proposal for the late Cenozoic geoynamic evolution of the western Mediterranean. Terra Nova 14, 93-100.

Gelabert, B., Sàbat, F., Rodríguez-Perea, A., Fornós, J., 2001. About the origin of the northern hemisphere Pàcific arcs. Bolletí de la Societat d'Història Natural de les Balears 44, 119-128.

Genç, Y., Yürür, M.T., 2010. Coeval extension and compression in Late Mesozoic–Recent thin-skinned extensional tectonics in central Anatolia, Turkey. Journal of Structural Geology 32, 623-640.

Göncüoglu, M.C., Köksal, S., Floyd, P.A., 1997. Post-collisional A-type magmatism in the central Anatolian crystalline complex: Petrology of the Idis Dagi intrusives (Avanos, Turkey). Turkish Journal of Earth Sciences 6, 65-76.

Guillaume, B., Martinod, J., Espurt, N., 2009. Variations of slab dip and overriding plate tectonics during subduction: Insights from analogue modelling. Tectonophysics 463, 167-174.

Gülyüz, E., Kaymakci, N., Meijers, M.J.M., van Hinsbergen, D.J.J., Lefebvre, C., Vissers, R.L.M., Hendriks, B.W.H., Peynircioğlu, A.A., Late Eocene evolution of the Çiçekdağı Basin (central Turkey): Syn-sedimentary compression during microcontinent–continent collision in central Anatolia. Tectonophysics (in press).

Gürer, A., and Bayrak, M., 2007. Relation between electrical resistivity and earthquake generation in the crust of West Anatolia, Turkey. Tectonophysics 445, 49-65.

Hacker, B.R., Peacock, S.M., Abers, G.A., Holloway, S.D., 2003. Subduction factory, 2, Are intermediate-depth earthquakes in subducting slabs linked to metamorphic

dehydration reactions?. Journal of Geophysical Research: Solid Earth 108 (B1), doi: 10.1029/2001JB001129.

Heuret, A., Funiciello, F., Faccenna, C., Lallemand, S., 2007. Plate kinematics, slab shape and back-arc stress: A comparison between laboratory models and current subduction zones. Earth and Planetary Science Letters 256, 473-483.

Heuret, A., Lallemand, S., 2005. Plate motions, slab dynamics and back-arc deformation. Physics of the Earth and Planetary Interiors 149, 31-51.

Houseman. G.A., Gubbins. D., 1997. Deformation of subducted oceanic lithosphere. Geophysical Journal International 131, 535-551.

Hyndman, R.D., Peacock, S.M., 2003. Serpentinization of the forearc mantle. Earth and Planetary Science Letters 212, 417-432.

Jolivet, L., Brun, J.-P., 2010. Cenozoic geodynamic evolution of the Aegean. International Journal of Earth Sciences 99, 109–138

Jolivet, L., Faccenna, C., Huet, B., Labrousse, L., Le Pourhiet, L., Lacombe, O., Lecomte, E., Burov, E., Denèle, Y., Brun, J.-P., and others. 2013. Aegean tectonics: Strain localisation, slab tearing and trench retreat. Tectonophysics 597, 1-33.

Jurdy, D.M., Stefanick, M., 1983. Flow models for back-arc spreading. Tectonophysics 99, 191-206.

Krantz, R.W., 1991. Measurements of friction coefficients and cohesion for faulting and fault reactivation in laboratory models using sand and sand mixtures. Tectonophysics 188, 203-207.

Koc□yiğit, A., Beyhan, A., 1998. A new intracontinental transcurrent structure: the Central Anatolian Fault Zone, Turkey. Tectonophysics 284, 317-336.

Lamb, H., 1994. Hydrodynamics (6th edition). Cambridge University Press. ISBN 978-0-521-45868-9.

Le Pichon, X., Angelier, J., 1981. The Aegean Sea. Philosophical Transactions of the Royal Society of London. Series A, Mathematical and Physical Sciences 3000, 357-372.

Leroy, M., Dauteuil, O., Cobbold, P.R., 2004. Incipient shortening of a passive margin: the mechanical roles of continental and oceanic lithospheres. Geophysical Journal International 159, 400-411.

Lister, G.S., Banga, G., Feenstra, A., 1984. Metamorphic core complexes of Cordilleran type in the Cyclades, Aegean Sea, Greece. Geology 12, 221-225.

Malinverno, A., Ryan, W.B.F., 1986. Extension in the Tyrrhenian Sea and shortening in the Apennines as result of arc migration driven by sinking of the lithosphere. Tectonics 5, 227-245.

Mantovani, E., Viti, M., Babbucci, D., Tamburelli, C., Albarello, D., 2001. Back arc extension: Which driving mechanism? Journal of the Virtual Explorer 3, 17-45.

Mantovani, E., Albarello, D., Tamburelli, C., Babbucci, D., Viti, M., 1997. Plate convergence, crustal delamination, extrusion tectonics and minimization of shortening work as main controlling factors of the recent Mediterranean deformation pattern. Annali Geofisica 40, 611-643.

McClusky, S., Balassanian, S., Barka, A., Demir, C., Ergintav, S., Georgiev, I., Gurkan, O., Hamburger, M., Hurst, K., Kahle, H., and others, 2000. Global Positioning System constraints on plate kinematics and dynamics in the eastern Mediterranean and Caucasus. Journal of Geophysical Research: Solid Earth. 105, 5695-5719.

Mercier, JL., Sorel, D., Vergely, P., 1989. Extensional tectonic regimes in the Aegean basins during the Cenozoic. Basin Research 2, 49-71.

Moix, P., Beccaletto, L., Kozur, H.W., Hochard, C., Rosselet, F., Stampfli, G.M., 2008. A new classification of the Turkish terranes and sutures and its implication for the paleotectonic history of the region. Tectonophysics 451, 7-39.

Molnar, P., Atwater, T., 1978. Interarc spreading and Cordilleran tectonics as alternates related to the age of subducted oceanic lithosphere. Earth and Planetary Science Letters 41, 330-340.

Nikolaeva, K., Gerya, T.V., Marques, F.O., 2010. Subduction initiation at passive margins: Numerical modeling. Journal of Geophysical Research: Solid Earth 115 (B3), doi: 10.1029/2009JB006549.

Peacock, S.M., 1993. Large-scale hydration of the lithosphere above subducting slabs. Chemical Geology 108, 49-59.

Pysklywec, R.N., Beaumont, C., Fullsack, P., 2000. Modeling the behavior of the continental mantle lithosphere during plate convergence. Geology 28, 655-658.

Regard, V., Faccenna, C., Bellier, O., Martinod, J., 2008. Laboratory experiments of slab break-off and slab dip reversal: insight into the alpine oligocene reorganization. Terra Nova 20, 267-273.

Regard, V., Faccenna, C., Martinod, J., Bellier, O., 2005. Slab pull and indentation tectonics: insights from 3D laboratory experiments. Physics of the Earth and Planetary Interiors 149, 99-113.

Regard, V., Faccenna, C., Martinod, J., Bellier, O., Thomas, J.-C., 2003. From subduction to collision: Control of deep processes on the evolution of convergent plate boundary. Journal of Geophysical Research: Solid Earth 108 (B4), doi: 10.1029/2002JB001943.

Reilinger, R., McClusky,S., Paradissis,D., Ergintav, S., Vernant, P., 2010. Geodetic constraints on the tectonic evolution of the Aegean region and strain accumulation along the Hellenic subduction zone, Tectonophysics 488, 22-30.

Ringwood, A.E., 1974. The petrological evolution of island arc systems. Journal of the Geological Society, London 130, 183–204.

Robertson, A.H.F. and Dixon, J.E., 1984. Introduction: aspects of the geological evolution of the Eastern Mediterranean. Geological Society, London, Special Publications 17, 1-74.

Rodkin, M.V. and Rodnikov, A.G., 1996. Origin and structure of back-arc basins: new data and model discussion. Physics of the Earth and Planetary Interiors 93, 123-131.

Royden, L.H., 1993. The tectonic expression slab pull at continental convergent boundaries. Tectonics 12, 303-325.

Scholz, C.H. Campos, J., 1995. On the mechanism of seismic decoupling and back arc spreading at subduction zones. Journal of Geophysical Research: Solid Earth 100, 22103-22115.

Sengör, A.M.C., Yilmaz, Y., 1981. Tethyan evolution of Turkey: A plate tectonic approach. Tectonophysics 75, 181-241.

Shemenda, A., Grocholsky, A.L., 1994. Physical modeling of slow seafloor spreading. Journal of Geophysical Research: Solid Earth 99, 9137-9153.

Tesauro, M., Kaban M. K., Cloetingh S.A.P.L., 2009. A new thermal and rheological model of the European lithosphere. Tectonophysics 476, 478-495.

Torsvik, T.H., Müller, R.D, Van der Voo, R., Steinberger, B., Gaina, C., 2008. Global plate motion frames: Toward a unified model. Reviews of Geophysics 46 (3), doi:10.1029/2007RG000227.

Turcotte, D.L. and Schubert, G., 1982. Geodynamics: Applications of continuum physics to geological problems. Wiley J, New York, 450 p.

van Hinsbergen, D.J.J. and Schmid, S.M., 2012. Map view restoration of Aegean–West Anatolian accretion and extension since the Eocene. Tectonics 31, TC5005, doi:10.1029/2012TC003132.

Weijermars, R., 1986. Flow behaviour and physical chemistry of bouncing putties and related polymers in view of tectonic laboratory applications. Tectonophysics 124, 325-358.

Figure captions

Fig. 1. Experimental apparatus and models. In experiments of Series A, wide piston (40 cm) advanced in direction perpendicular to continent-ocean boundary (COB). In Series B, wide piston (40 cm) advanced in direction parallel to COB. In Series C, narrow piston (20 cm) compressed continental plate in direction parallel to COB.

Fig. 2. Surface views of Series A, B and C before piston displacement (upper part of figure), and of Series A after deformation (lower part), for piston velocities of 0.1 cm/h (A1), 0.5 cm/h (A2) or 2.5 cm/h (A3).

Fig. 3. Surface views (photographs and their interpretations) of Model 7 (Series B) after 3, 6, 9, 12, 15, and 18 h. Piston moved at 0.5 cm/h, then stopped after 12 h (6 cm of shortening).

Fig. 4. Surface views (photographs and their interpretations) of Model 8 (Series C) after 3, 6, 9, 12, 15, and 18 h. Piston moved at 0.5 cm/h, then stopped after 12 h (6 cm of shortening).

Fig. 5. Surface views (photographs and their interpretations) of Models 5, 7 and 9 (Series B, upper part of figure) and Models 4, 6 and 8 (Series C, lower part of figure) after 12h of shortening at 0.5 cm/h (6 cm of shortening) and for three values of density ratio (R) between oceanic plate and continental plate.

Fig. 6. Top: change in surface area (as % of total area) with time, for each of continental plate, oceanic plate and piston of Model 5 (a), Model 7 (b) and Model 9 (c) of Series B. Bottom: change in surface area (%) with time for continental plate of each of Models 5, 7 and 11 (Series B, left, e) and Models 4, 6 and 8 (Series C, right, f). In all graphs, thick grey vertical line marks moment when piston stopped.

Fig. 7. Change in surface area (%) with time, for continental plates of 6 models, versus density ratio between oceanic plate and continental plate. Numbers in brackets indicate density ratios between oceanic plate and asthenosphere.

Fig. 8. Map of Aegean Sea, Anatolia and surrounding areas, showing main structural features and area of Late Oligocene to present-day extension (GPS data from Reilinger et al., 2010). Inset (top left) shows location with respect to Europe and Africa and the main tectonic elements of Turkey. Abbreviations in figure are KFZ, Kžrklareli Fault Zone; NAFZ, North Anatolian Fault Zone; WAGS, West Anatolian graben System; EFZ, Eskis¸ehir Fault Zone; FBFZ, Fethiye Burdur Fault Zone; IASZ, I™zmir Ankara Suture Zone; EAFZ, East Anatolian Fault Zone; DSFZ, Dead Sea Fault Zone; KTJ, Karlžova Triple Junction. (modified from Gürer and Bayrak, 2007).

Table 1. Values of experimental parameters for each of models 1 to 12 (h for layer thickness, ρ for density and μ for viscosity).

Table 2. Characteristic values of parameters in nature and models and corresponding model ratios.

Table 1

	Series A			Series B			Series C		
	Velocity test R=1.3			R = 1.1	R = 1.3	R = 1.4	R = 1.1	R = 1.3	R = 1.4
MODEL	**1**	**2**	**3**	**5**	**7**	**9**	**4**	**6**	**8**
Continental Plate									
h sand (cm)	0,5	0,5	0,5	0,5	0,5	0,5	0,5	0,5	0,5
ρ sand (g/cm³)	1,32	1,32	1,32	1,32	1,32	1,36	1,36	1,32	1,36
h silicone (cm)	2,5	2,5	2,5	2,5	2,5	2,5	2,5	2,5	2,5
ρ silicone (g/cm³)	1,23	1,23	1,23	1,18	1,25	1,175	1,346	1,25	1,175
μ silicone Pa s	47200	47200	47200	32800	50000	46000	31700	56807	46000
Oceanic Plate									
h sand (cm)	0,3	0,3	0,3	0,3	0,3	0,3	0,3	0,3	0,3
ρ sand (g/cm³)	1,56	1,56	1,56	1,56	1,56	1,56	1,56	1,56	1,56
h silicone (cm)	0,7-1,2	0,7-1,2	0,7-1,2	0,7-1,2	0,7-1,2	0,7-1,2	0,7-1,2	0,7-1,2	0,7-1,2
ρ silicone (g/cm³)	1,67	1,67	1,67	1,336	1,67	1,655	1,557	1,67	1,655
μ silicone Pa s	153000	153000	136000	66500	153000	78500	26800	136000	78500
Honey									
ρ (g/cm³)	1,432	1,432	1,432	1,432	1,432	1,432	1,37	1,432	1,432
μ Pa s	10	10	10	10	10	10	10	10	10
Piston Velocity									
cm/h	0,1	0,5	2,5	0,5	0,5	0,5	0,5	0,5	0,5
Buoyancy number, F									
	--	--	--	0,26	1,32	2,48	7,81	1,49	2,48

Table 2

Parameter		Nature	Models	Nature/model
	g (m/s)	9.81	9.81	1.00
	Length	30 km	1 cm	3.0×10^{6}
	Time	1 Ma	1 h	6.4×10^{9}
Thickness (cm)				
	Oceanic lithosphere	7.2×10^{6}	0.7 to 1.2	7.5×10^{6}
	Contiental lithosphere	1.5×10^{7}	3.00	5.0×10^{6}
Density (kg/m³)				
	Oceanic plate	3300	1670	1.98
	Continental plate	3220	1250	2.58
	Asthenosphere	3300	1432	2.30
Viscosity (Pa.s)				
	Oceanic plate	2.5×10^{20}	2.7×10^{4}	9.3×10^{15}
	Continental plate	2.5×19^{22}	5.7×10^{4}	4.4×10^{17}
Velocity				
		1.5 cm/y	0.5 cm/h	3.0×10^{3}

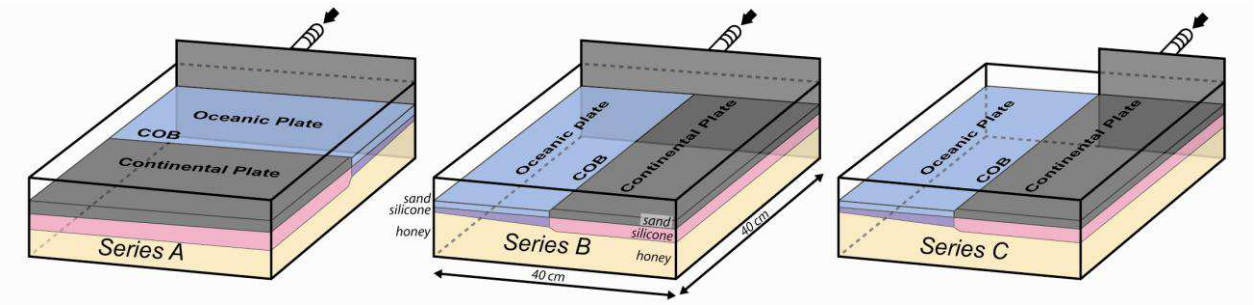

Figure 1

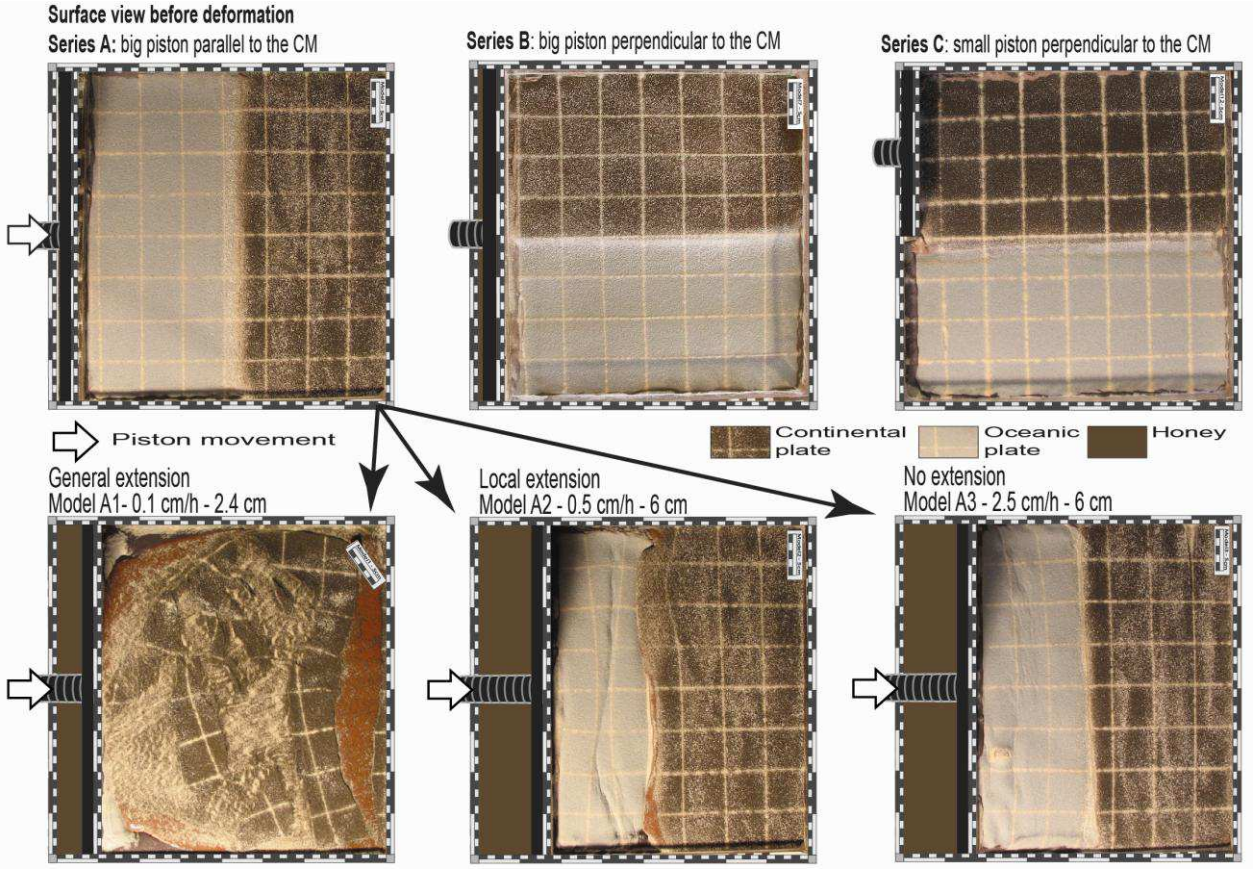

Figure 2

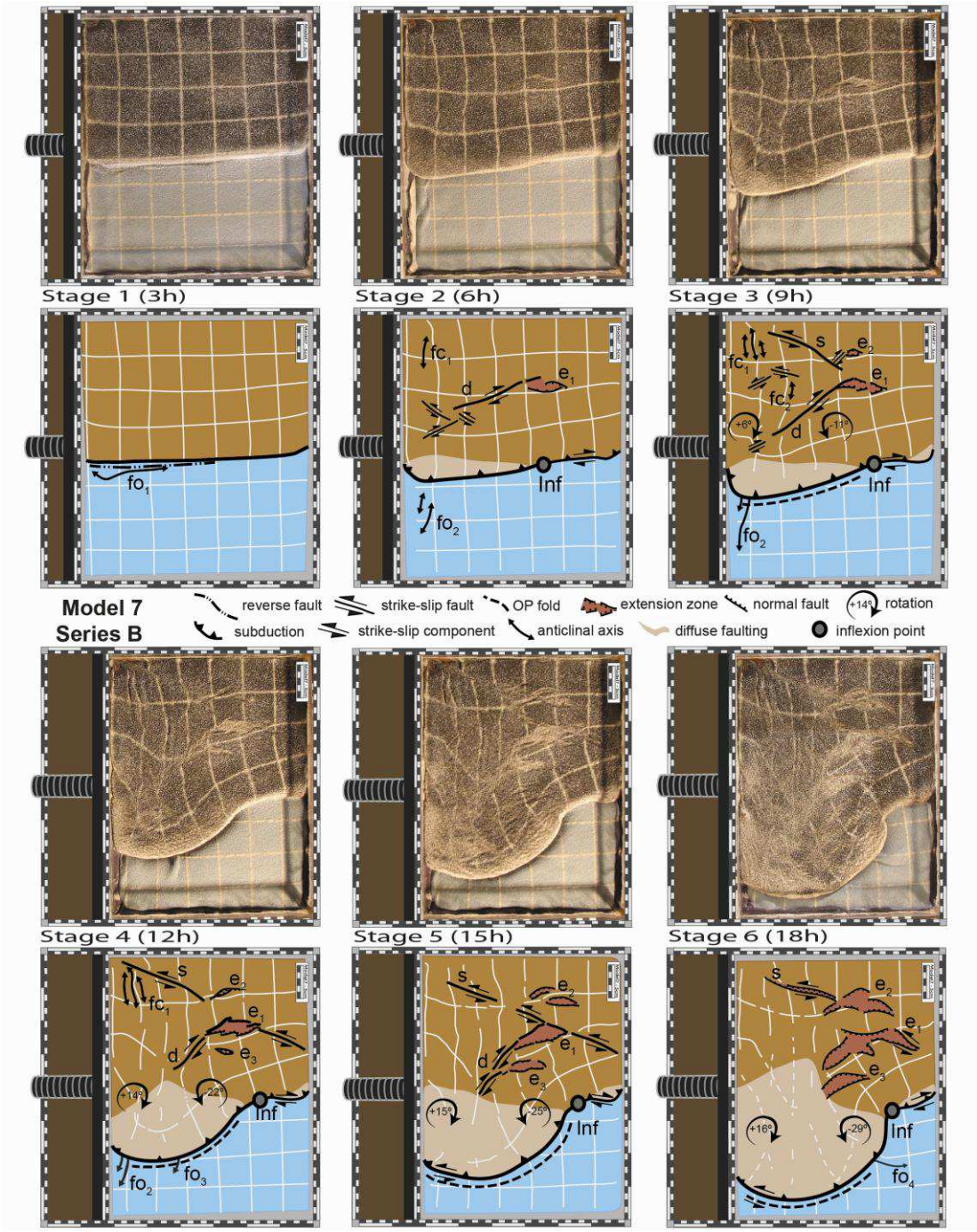
Stage 1 (3h)
Stage 2 (6h)
Stage 3 (9h)
Model 7
Series B
reverse fault
subduction
strike-slip fault
strike-slip component
OP fold
anticlinal axis
extension zone
diffuse faulting
normal fault
rotation
inflexion point
Stage 4 (12h)
Stage 5 (15h)
Stage 6 (18h)
Inf
fc1
fc2
fo1
fo2
fo3
fo4
d
s
e1
e2
e3

Figure 3

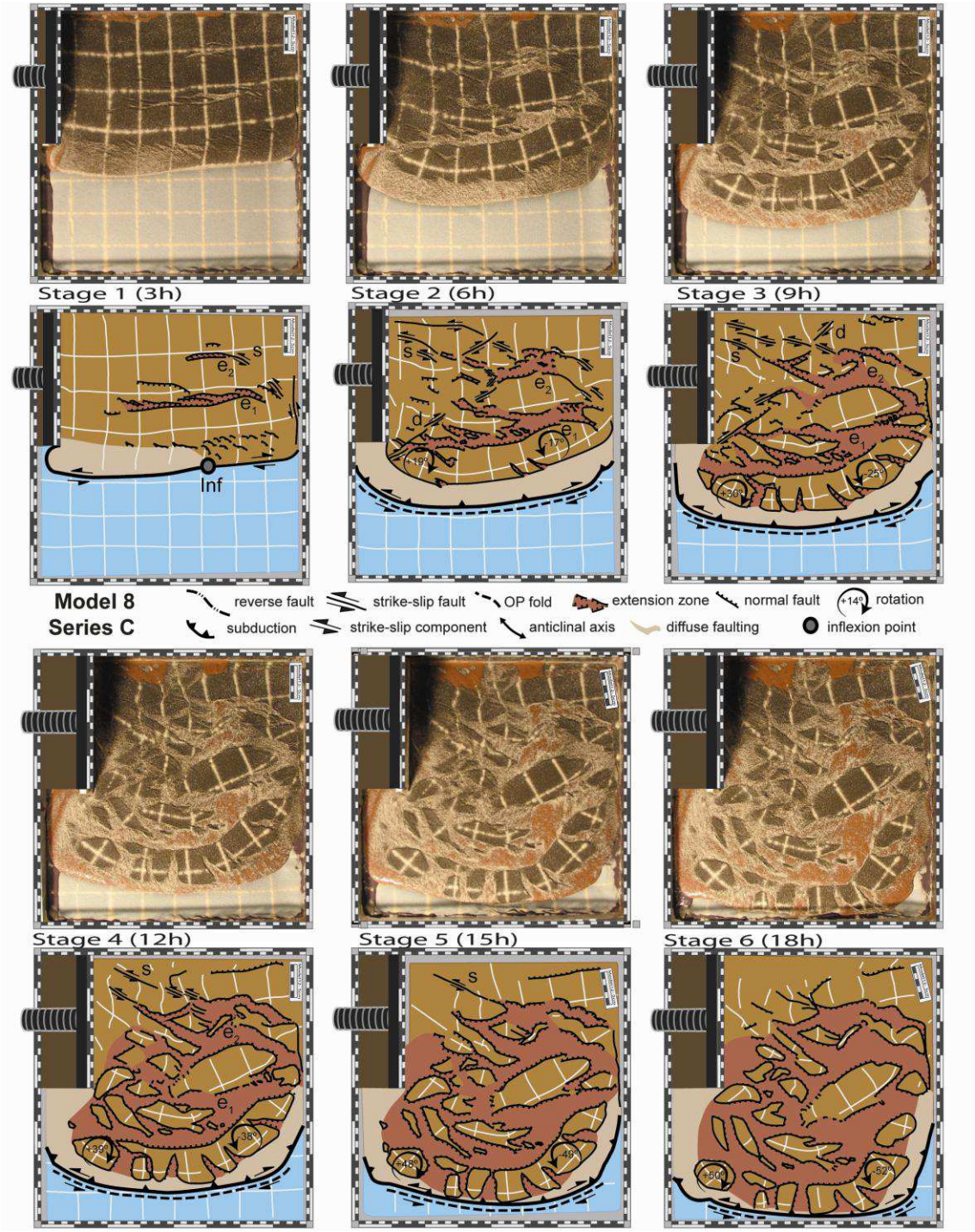
Stage 1 (3h)
Stage 2 (6h)
Stage 3 (9h)
Inf
Model 8
Series C
reverse fault
strike-slip fault
OP fold
extension zone
normal fault
rotation
subduction
strike-slip component
anticlinal axis
diffuse faulting
inflexion point
Stage 4 (12h)
Stage 5 (15h)
Stage 6 (18h)

Figure 4

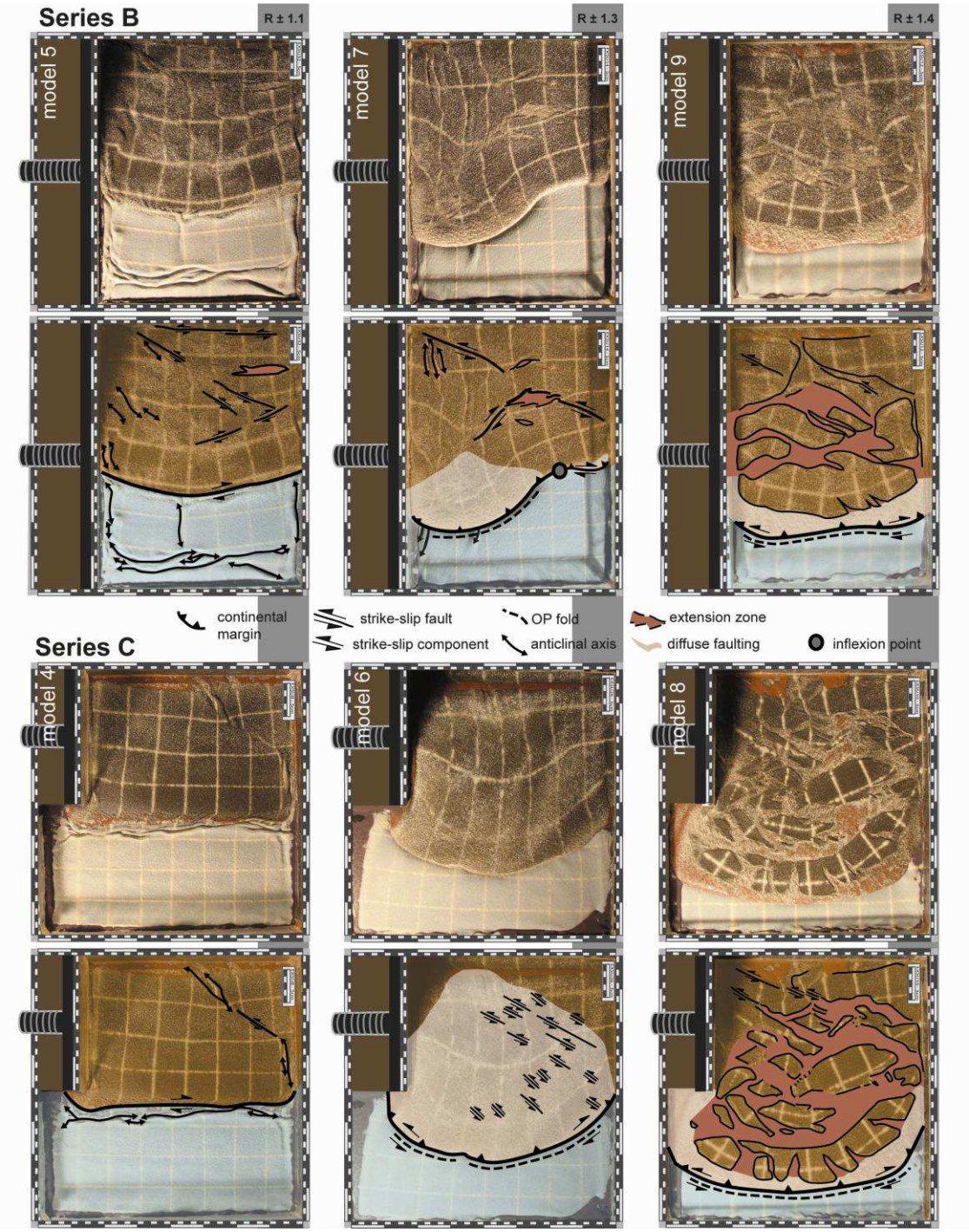

Figure 5

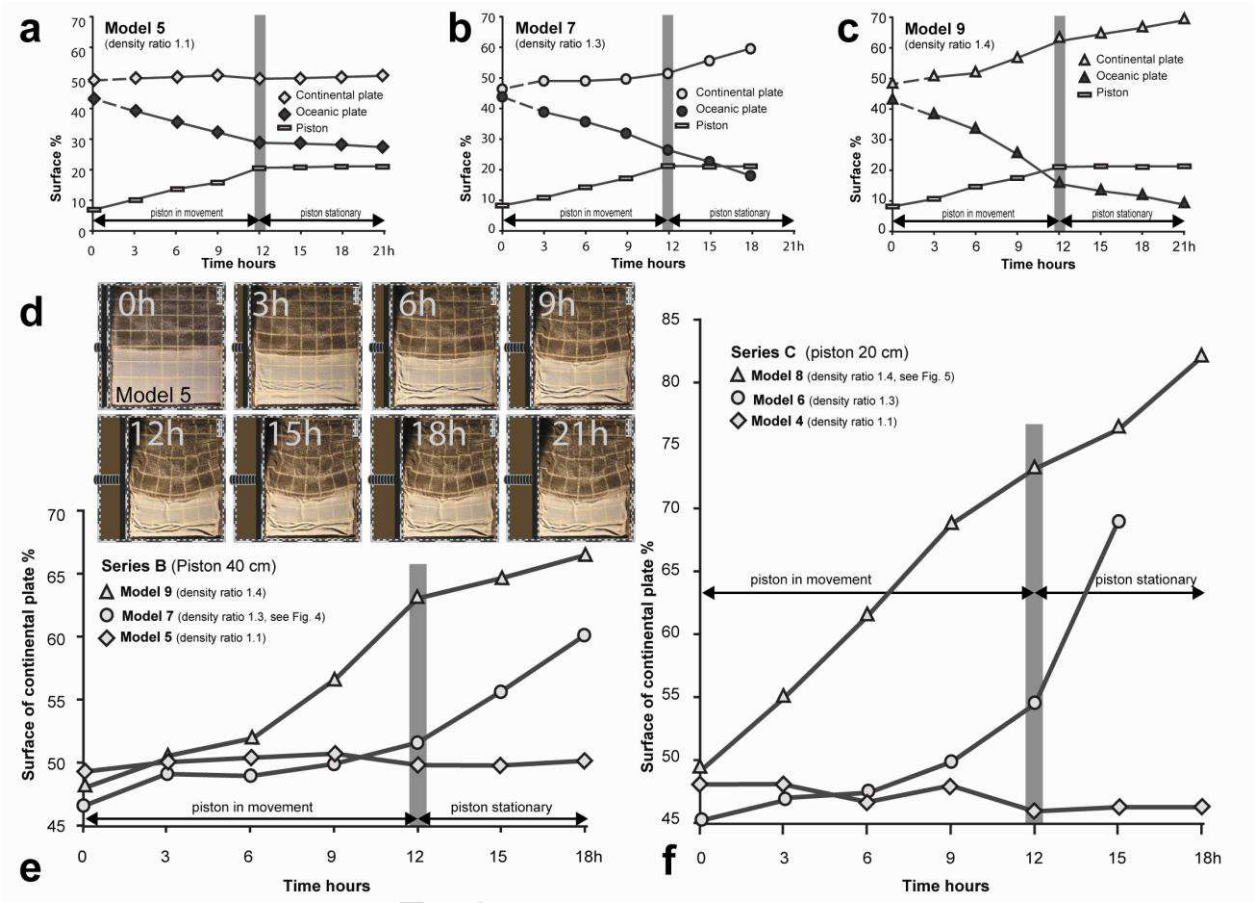

Figure 6

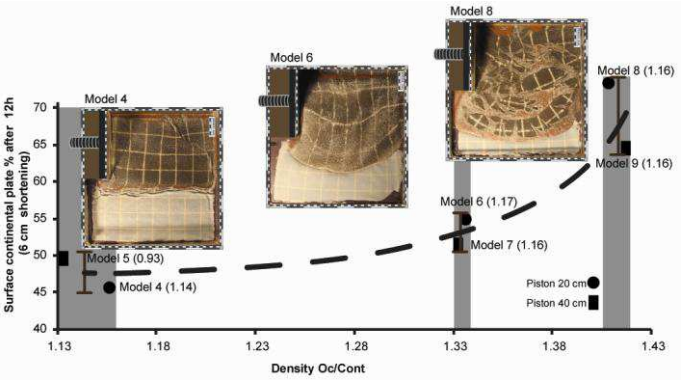

Figure 7

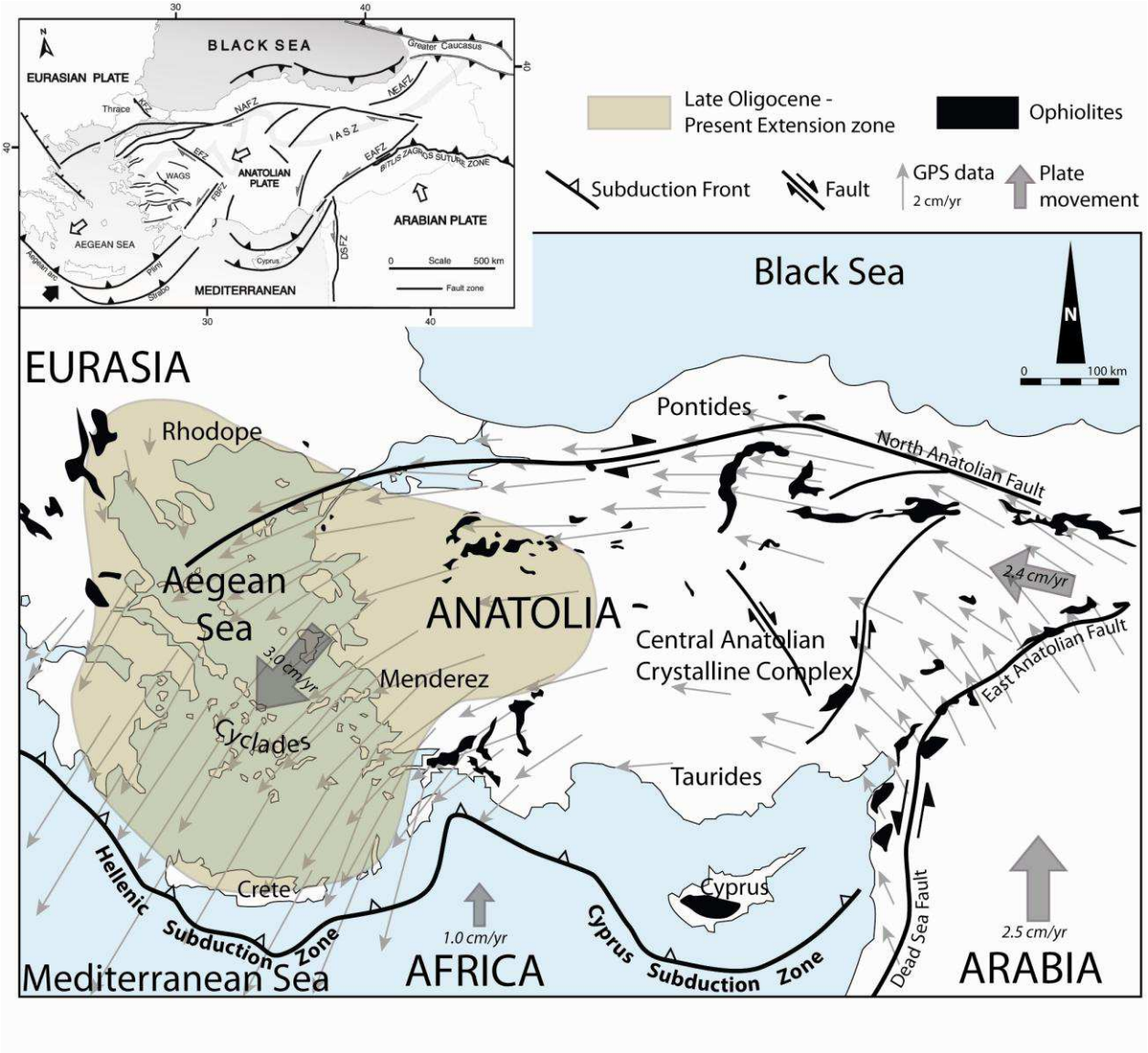

Figure 8

Highlights

- Models consisted on oceanic and continental plates floating on asthenosphere.
- We tested deformation velocity and density ratio (oceanic vs continental plate).
- We examine the factors generating extension during subduction.
- The density ratio is a key factor to facilitate extension during subduction.
- We propose an application to the Anatolian system.